Dust Source and Susceptibility Map in Iran and Iraq: Application of Remote Sensing and Machine Learning Techniques

Sima Pourhashemi
Hakim Sabzevari University
Mohamadali Zanganeh asadi (ma.zanganehasadi@hsu.ac.ir)
Hakim Sabzevari University
Mahdi Boroughani
Hakim Sabzevari University
Hossein Azadi
Ghent University: Universiteit Gent

Research Article

Keywords: Dust Source, Susceptibility Map, Remote Sensing, Machine Learning Techniques

Posted Date: June 3rd, 2022

DOI: https://doi.org/10.21203/rs.3.rs-1613035/v1

Abstract

The dust storm is one of the major environmental problems that has affected many arid regions of the world. This research aimed to investigate the factors affecting the dust source area (DSA) and to prepare a sensitivity map in Khuzestan province in Iran and Al-Basrah and Maysan provinces in Iraq. For this research, Remote Sensing (RS) techniques and machine learning techniques, including Multivariate Adaptive Regression Spline (MARS), Random Forest (RF), and Logistic Regression (LR), were used for dust source identification and susceptibility map. One hundred fifty-two DSA for a period of 2005–2020 were identified in the study area. Seventy percent of sources were selected for the Dust Source Susceptibility Mapping (DSSM) (training dataset), and thirty percent of sources were used for model validation. Consequently, six factors including soil, lithology, slope, and normalized vegetation differential index, geomorphology, and land use units were prepared as independent and effective variables on the DSA. The results of all three models indicated that land use had the most impact on the creation of DSA. The validation results of these models using the training data showed sub-curves of 0.92, 0.86, and 0.76 for the RF, MARS, and LR models, respectively. Also, the outcome showed that the RF model had the best performance in comparison with MARS (AUC = 0.89) and LR (AUC = 0.78) methods. The results showed that in all three models, high and very high susceptibility classes generally covered a large percentage of the case study. The highest percentage of dust source points was also in this susceptibility category. The results of this study can be useful for planners and managers to control and reduce the risk of negative dust consequences.

1. Introduction

Dust storms as a catastrophic weather phenomenon have adverse effects on the quality of the environment and cause significant damage to health, agricultural products, and, thus, the economy (Guo et al., 2018; Liu et al., 2020). Strong winds are the greatest important cause of dust events, and soil surface properties such as vegetation distribution, surface roughness, soil texture, and moisture have important effects on dust emission. (Shaheen et al., 2020). The dust source points are located in areas with less than 300 mm of rainfall in the world (Wang et al., 2016; Dousari et al., 2017; Kandakji et al., 2021). When wind speeds in dry areas and deserts exceed the wind erosion threshold (8 meters per second), soil particles rise and dust storms occur (Namdari et al., 2021). Dust particles can reach a height of six km above the ground and be transported up to a distance of 20,000 kilometers (Taheri et al., 2020). Dust storms in arid and semi-arid regions affect the amount of solar radiation, air pollution, horizontal vision, enzymatic activities, agricultural lands, and human health (Boroughani et al., 2022; Martinich et al., 2019; Yang et al., 2018). In recent years, due to drought and Land Use Change (LUC), the frequency of days with dust storms has increased significantly, which causes adverse biological effects and extensive damage to agriculture, industry, and society. The combined development of this event along with the accelerated trend of development, industrialization, and population growth in urban areas has doubled the environmental tensions (Shaheen et al., 2020; Boloorani et al., 2020). Dust storms are happening in arid land in the world, especially in North Africa and the Middle East (Yu et al., 2016; Francis et al., 2021).

The result of dust storms is the reduction of visibility and serious environmental, socio-economic, and health issues (Middleton, 2017). The Middle East has severe environmental challenges such as climate and environmental changes caused by human activities (Karimi and Samadi., 2019). The root cause for the increase in dust in the region is the severe destruction of natural resources due to extensive exploitation, drying of wetlands, dam construction, and the continuation of the drought in the last decade (Cao et al., 2015). Identifying areas of dust origin using remote sensing techniques is one of the main important methods in the world (Jiao et al., 2021). Many research has an emphasis on determining dust detection using RS techniques. In most of these studies, MODIS images and dust detection indices (BTD2931, BTD3132, NDDI, parameters D and DEP) were used to identify dust in the Saharan Desert (Schepanski et al., 2012; Feuerstein and Schepanski, 2019), Chihuahuan Desert (Baddock et al., 2016), Iran (Rahmati et al., 2020), Khorasan Razavi Province, Urmia Lake and Sistan watershed, Iran (Boroughani et al., 2019, 2020, 2021), Middle East (Namdari et al., 2018), India (Soni et al., 2018), USA and Middle East (Miller, 2003), and Southwestern North America (Lee et al., 2009). Data mining is an important method for mapping environmental and natural hazards, it is a way to find new and useful data from lots of information. (Gholami et al., 2020). Numerous studies (e.g., Hong et al., 2016; Dube et al., 2014; Manap et al., 2014; Boroughani et al., 2020; Lee et al., 2021) have used a data mining approach using different algorithms and models to identify and generate susceptibility maps of dust, landslide, groundwater, fire, flood, and gall erosion centers. The concept of data mining includes algorithms and methods that are used to extract information from important data (Akbari et al, 2017).

Considering the intensity and the large number of dust storms in the case study (Iran and Iraq) and their importance, the purpose of this study is to identify dust sources and generate a susceptibility map using these algorithms. The main aims of this study are (i) identifying the sources of dust with remote sensing techniques; (ii) generating dust susceptibility mapping using MARS, RF, and LR algorithms; (iii) comparing the accuracy of model outputs using statistical evaluation criteria; (iv) and determining the importance of each ventilation agent in the potential of the dust source.

2. Methodology

2.1 Setting of the study

The research area covers Khuzestan province in Iran and Al-Basrah and Maysan provinces in Iraq with an area of 99494.38 km^2 (Fig. 1). The highest altitudes in the region of 3676 and the lowest altitudes are −37 m. Al-Hawizeh / Al-Azim swamps, located on the border between Iraq and Iran, are known as one of the main dust sources in Iran. According to Javadean et al. (2019), Al-Howizeh/Al-Azim marshes are one of the three greatest important dust sources in the city of Ahvaz. Wetlands in Iran in the last decade due to oil extraction around Al-Azim, have dried up and created a source of dust (Arkian, 2017). Several other factors, including climate change, drought, wars in the region and military operations, surface water control, river diversion, and dam construction projects, have contributed to the destruction of these wetlands and the emergence of their surface as dust source (Cao et al., 2015; Rashki et al., 2021). The

Khuzestan Plain, which forms a large part of Khuzestan Province in southwestern Iran, contains much small dust sources. Approximately nine percent of the Khuzestan plain is the potential of producing dust, part of which is sensitive to the dust source of the Al-Azim dried-up swamp (Heidarian et al., 2018(. These source areas contain degraded pastures, abandoned rainfed farmlands and irrigation fields, and temporary salt lakes. Among these salt lakes, we can mention Maleh Playa, Sabzeh Zohreh Sharghi, and Sabkha Karun Gharbi (Abyat et al., 2019).

Figure 1. Location of the research area

In the present research, the flowchart (Fig. 2) shows two main stages. At first, DSA was determined using satellite images (MODIS) and dust detection indices. In the second stage, sensitivity maps were prepared by six environmental forecasters and the DSA extracted from satellite images and three machine learning algorithms, namely logistic regression, random forest and MARS model were examined. In the following, the working method and dataset are explained in detail.

Figure 2. Flow chart for preparation of dust susceptibility maps using LR, MARS, and RF models

2.2 Dust Source Identification

In this study, MODIS sensor images from Terra and Aqua satellites were collected (Vickery and Eckardt, 2013). Initially, the days of dust occurrence in the years 2005 to 2020 were determined using meteorological data, such as visibility less than 2000 m, wind speed above 7 m per second, and cloudy conditions. Then, the days when the occurrence of dust coincided with the imaging were determined, and finally, 31 MODIS sensor images were used by the Terra satellite related to the selected dust days from 2005 to 2020.

MODIS images were selected due to several advantages including the free access, the high spatial resolution (LAADS Alerts, 2021), and the wide view (Hahnenberger and Nicoll, 2014; Lee et al., 2021). The method used to identify and detect DSA is the Dust Detection Products (DEP) method or the Miller method, which was calculated for all satellite images (Miller, 2003). Finally, false-color combinations were used to identify dust storms. These were according to the DEP plus bands 3 and 4 of MODIS images. The false-color combinations included DEP (Miller, 2003), B4, and B3. A Gaussian columnar model was used to detect dust. This technique is developed on a cone of dust diffusion viewed in the processed MODIS images, where the apex shows the source of the dust (Walker et al., 2009; Lee et al., 2009).

2.3 Dust source effective factors

Quantifying the relative significance of the factors influencing the area's dust source is essential to understanding the dust cycle (Kok et al., 2018). To prepare the potential map of the DSA, after preparing the distribution map of the DSA, six factors including soil maps, lithology, slope, vegetation index (Normalized Difference Vegetation Index), geomorphology units, and land use were considered. These factors play the most important roles in creating DSA (Kandakji et al., 2020).

Dust storms are more likely to occur in regions with erosion-sensitive lithological units than in areas with resistant units (Francis et al., 2017). Lithology classes have significant effects on dust storms and occur more in regions susceptible to lithology than in regions with dust storm-resistant units (Francis et al., 2017). To prepare the geological map of the research area, the world geological map at a scale of 1: 250,000 was used. Also, lithological units were obtained from the map in 6 classes Siltstone and Marne, dolomitic limestone and clay, limestone, conglomerate, river sediments, and wind sand (Fig. 3a). Dust storms and the amount of dust raised to depend on the physical characteristics of the soil (Alilou et al., 2019; Rahmati et al., 2020). Vegetation-free soils are erosion-sensitive areas with high dust production capacity (Gholami et al., 2020). In this study, 6 main types of floors including Clay-Loam, Loam, Loamy-Sand, Sandy-Loam, Sand, and Salty-Clay were identified (Fig. 3b).

Plain and flatlands with low slopes have a better potential for dust generation and wind erosion than steep lands. In these regions, the wind quickly reaches the threshold of wind erosion and leads to dust storms (Wu et al., 2016). Using the DEM of 30 m, the slope map of the research area was readied in six classes. (Fig. 3c). In many studies (e.g., An et al., 2018; Lee and Sohn, 2011), by analyzing the spatial and long-term changes of vegetation, a negative relationship between vegetation and the number of dust storms have been identified. The vegetation can absorb wind energy, increase ground roughness, and protect soil from wind erosion (Feng and Janssen., 2018). The Normalized Vegetation Differential Index (NDVI) was used to prepare the vegetation map of the area. For this goal, ETM $^{+}$ images of the Landsat 8 satellite (related to 2019) were used. The NDVI map was prepared using Eq. 2.

$$\mathrm{NDVI} = \frac{\mathrm{NIR} - \mathrm{Red}}{\mathrm{NIR} + \mathrm{Red}} \qquad (2)$$

The NIR indicates infrared and the Red indicates the red band. The NDVI was divided into 3 vegetation classes including − 0.0196-0, 0-0.025, and 0.025 < throughout the study area (Fig. 3d).

Land use is strongly associated with dust storms; for example, lack of vegetation and degraded soil crust has a greater capacity to produce dust (Goossens and Buck, 2014). The land use map was prepared using Landsat 8 satellite images for summer 2018 due to the highest amount of dust occurring in this period. The land use map was classified into the Agriculture land. Bare land, Forest, Marshland, Residential Area, Shrub Cover, Sparse Shrub Cover, and Wetland. (Fig. 3e).

Soil particles released into the air are closely related to the geomorphological characteristics of DSA. (Lee et al., 2021). To prepare the map of geomorphology units, first, the required map was prepared using slope and topographic maps with an accuracy of 1: 50,000 and the geology of the research area. In the next step, after interpreting the satellite images of Google Earth and Landsat 8 in 2017, more detailed information was extracted and transferred to the initial map. Finally, the map of the geomorphological units of the region in six classes was prepared (Fig. 3f).

Figure 3. Map of effective factors of dust source

2.4 Modeling

To examine alignment make a preliminary study between among independent variables, multi-collinearity was analyzed. If there are several lines between independent variables, the error increases, and the accuracy of the model prediction decreases (Park, 2017). Two indicators, A tolerance of less than 0.1 (≤ 0.01) and a variance coefficient of ≥ 10 indicating alignment were used to examine the alignment between the independent variables (O'brien, 2007).

The first step for modeling is to prepare an educational data set and validation (Boroughani et al, 2020). To perform the modeling, first using the stratified random sampling method (Lee et al., 2021), dust source was divided into two groups of 70% (106 dust sources) for modeling and 30% (46 dust sources) for evaluation (Validation). To analyze the sensitivity of the DSA using data mining algorithms, and the number of DSA in the area, the number of points without the DSA was randomly extracted. In the next step, the data related to the effective factors in the area of dust source and source distribution map were entered into the R software, and LR, MARS, and RF algorithms were used using packages (glm; earth, random forest etc.). The dust source susceptibility was then calculated for each pixel in the study area. Finally, the results were transferred to the ARC MAP 10.5 environment to produce a dust susceptibility map. A description of the algorithms used is given below.

2.5 Logistic Regression (LR)

LR is a nonlinear mathematical model for determining the relationship between a binary dependent variable and several independent variables (Crawford et al., 2021). In this research, using LR, the most effective factors in DSA were investigated. The output of the model should have coefficients between 0 and 1, which through logit theory gives probabilities higher than 0.5 value of 1 (affecting the DSA) and less than 0.5 value of zero (without the effect of the DSA) (Martinez-Garcia et al., 2011; Chen and Chen., 2021).

The logistic model in the simplest form can be expressed as Eq. 3:

$$P = \frac{1}{1+e^{-z}} \quad (3)$$

Where P is the possibility of an occurrence of an event (DSA), the value of which fluctuates from 0 to 1 in an S-shaped curve, Z is defined as an equation (linear logistic model) whose value fluctuates from -∞ to +∞ (Wang et al., 2021). Eq. 4 is stated (Nhu et al., 2020).

$$Y = \text{Logit}(p) = \ln\left(\frac{p}{1-p}\right) = C_0 + C_1X_1 + C_2X_2 + \cdots + C_nX_n \quad (4)$$

P: Probability of an occurrence (probability of occurrence of DSA): The so-called odds ratio or probability, the width of the source or a constant coefficient, and C1, C2,… Cn, the coefficients of the independent variables (X1, X2,…, Xn). This model analyzes the presence or absence of dependent variables (DSA) to independent variables (Crawford et al., 2021).

2.6 Random Forest (RF) model

RF is one of the best learning algorithms (Schonlau and Zou, 2020). For many datasets, it performs high-accuracy classification (Lee et al., 2017) and another positive feature is that it works very well with huge data records (Jiang et al., 2021). RF classification was performed initially on educational information and then on validation confirmation information (Schonlau and Zou, 2020; Quevedo et al., 2021). Finally, the model with the lowest Out of Bag (OOB) error is chosen. To determine the priority of the effect of each of the effective factors in RF, two factors of mean reduction accuracy and Gini mean reduction were used (Wu et al., 2021).

2.7 Multivariate Adaptive Regression Spline model (MARS)

MARS is one of the local nonparametric models first proposed by Friedman (Wang et al., 2021). In this method, regression models create flexibility for dividing the response space into intervals of input variables and fitting a base pan (spline). (Wang et al., 2020; Friedman, 1991). This method is based on functions called base functions (functions that are used to display information in one or more variables), which are defined for each variable as follows:

$$Y = \max(0, x-t) \text{ and } Y = \max(0, t-x) \qquad (5)$$

which is t reached a Knot and is a threshold value. These functions are called spline functions, where t pairs are reflected in a node. The general shape of the MARS model is defined as follows (Roy et al, 2020):

$$\hat{Y} = f(X) + c_0 + \sum_{k=1}^{M} c_k B_k(X) \qquad (6)$$

In Eq. 6, Y is the value of the objective parameters defined by the function f (X), B_k which are the base function, and the coefficients c_k which are determined by minimizing the sum of the remaining squares. In the second step, the basic functions that are less important and effective in estimating are removed. Finally, the best model is chosen based on the minimum criterion called Generalized Cross-Validation (GCV). GCV is used to identify the sub-models that have the least effect on modeling.

Suppose $GCV_k$the value GCV for the k model is in the elimination phase the GCV on which the best adaptive multiple spline regression models is selected is also as follows (Martinello et al., 2021; Hassangavyar et al., 2020):

$$GCV_k = \frac{1}{n}\sum_{i=1}^{n}\left(y_i - \hat{f}_k\left(x_i\right)\right)^2 / \left(1 - \frac{C(k)}{n}\right)^2 \quad (7)$$

That $\hat{f}_k$ the model is estimated in step k of the regression elimination stage and $\lambda . m$ + Number of model sentences in step k = $C(k)$

m represents the number of nodes of the linear functions in the model and λ is called the smoothing parameter and in practice is usually chosen between 2 and 4.

2.8 Evaluation of dust source susceptibility map

One of the most important parts of modeling is the validation of predicted results (Shano et al., 2021). In this research, all identified DSA were separated into two parts: One is for training (70% DSA) and the other is for validation (30% DSA). DSAs were selected based on random logic for training and validation of models. The ROC-AUC (r receiver-operating characteristic area below the curve) and RMSE (the root mean square error) were used to evaluate the accuracy of the statistical model. The most ideal model has the highest subsurface level and its value is between 0.5 to 1 (Nandi and Shakoor., 2009). The closer the surface below the curve is to one, the more accurate the zoning map (Hao et al., 2020). Qualitative-quantitative correlation should be below the curve and estimation of the 0.9-1, excellent; 0.8–0.9, very good; 0.7–0.8, good; 0.6–0.7, average; 0.5–0.6, weak is suggested (Arabameri et al., 2021). The ROC curve was used in this study to appraise the performance of the generated susceptibility map. However, some studies suggest that model performance evaluation using a factor such as AUC may not be appropriate because in some cases high AUCs may not guarantee the high accuracy of spatial predictions (Chaudhary et al., 2021). For this case, RMSE measurements are also used as additional criteria for evaluating model predictions and supporting decisions in model selection.

3. Result And Discussion

3.1 Dust source Identification

A total of 152 DSA (77 in Iran and 75 in Iraq) were identified throughout the examined region, (Fig. 4). The analysis was based on the results of previous studied that used remote sensing techniques for identifying DSA in some parts of the world (Walker et al., 2009; Miller., 2003; Miller, 2012; Hahnenberger and Kathleen, 2014; Boroughani et al., 2020). These studies identified dust storm sources using dust detection products (DEP) and dust enhancement indicators. Figure 5 shows dust detection from the MODIS FCC satellite imagery over the case study on 17 June 2008.

Figure 4. Distribution of dust sources points identified

Figure 5. Dust detection in the case study from the MODIS satellite Imagery with FCC (R: DEP, G: B4, B: B3)

The results of the multilinear test (Table 1) confirmed that there was no agreement between the effective factors (independent variables), and therefore all layers were used for modeling.

Table 1
Multicollinearity diagnostic indices for effective factors.

factors	Tolerance	VIF
Slope	.236	4.239
Geomorphology	.241	4.144
Land use	.793	1.262
Lithology	.456	2.191
Soil	.539	1.855
NDVI	.454	2.201
Source: Study findings		

3.2 Dust source susceptibility modeling

The DSSM was done in the research area based on the coefficients obtained for independent variables through the model implementation. The results of the logistic regression model to investigate the most important factor affecting the creation of DSA are presented in Table 3. Based on the results, land use has had the greatest impact on the creation of DSA. Geomorphology, soil, and vegetation index are affected in the following categories. Negative coefficients indicate the inverse relationship of the dependent variable (DSA) with independent variables. Negative coefficients do not indicate a lack of correlation, but it means a weaker correlation than other factors. The lithological factor has the least impact on the formation of these DSA. To evaluate the validity of the model and to evaluate the fit of the estimated pattern, the Hosmer and Lemeshow test and Negelkerke coefficient were used. In the Hosmer and Lemeshow test, if the significance of the obtained model is more than 0.05, the model is valid (Gomila, 2021). Given that the probability of the Hosmer and Lemeshow test statistic is 0.158, which is greater than 0.05, this value indicates the adequacy of the data for the suitability of the model.

Table 2
Model Summary

-2 Log likelihood	Cox & Snell R Square	Nagelkerke R Square
471.3[a]	.43	.42
Source: Study findings		

Table 3
Coefficients of independent logistic regression statistical analysis.

Variables	B	Wald	Sig.	Exp(B)
Soil	− .599	7.161	.007	.550
geomorphology	.674	7.923	.005	1.963
Land use	− .933	25.653	.000	.393
Lithology	− .163	.782	.037	.849
Slope	− .383	2.946	.086	.682
NDVI	− .270	.960	.032	.763
Source: Study findings				

In the Nagelkerke coefficient of determination method, the closer this value is to one, the more the model corresponds to reality (Zhang et al., 2021). The value of Cox and Snell is 0.4312 and this value is significant in practice. The results of this model are shown in Table 2.

The results of the relationship between DSA and effective factors using the RF model are shown in Table 5 and Fig. 6. As previously mentioned, two factors of the Gini significance index and decreasing mean accuracy were used to determine the priority of each of the effective factors in creating DSA. Figure 6 shows the results of prioritizing the effective variables for the RF model using two criteria of decreasing mean accuracy and Gini significance index. The results of both criteria showed that the three factors of land use, soil, and geomorphology have the greatest impact on the creation of DSA. In most studies conducted in most parts of the world, these three factors have been identified as the most effective factors in creating DSA (Genuer et al., 2017; Giang et al., 2020; Ebrahimi-Khusfi et al., 2021). Boroughani et al. (2020) determined that land use and geomorphology had a major influence on the DSA in Khorasan Razavi province in Iran.

Table 4
Confusion matrix for random forest model: 0 = dust source absents, 1 = dust source present

	Predicted		
	0	1	Class error
Actual			
0	97	9	0.084
1	11	95	0.15
Source: Study findings			

Table 5
Results of determining the degree of importance of effective variables in the MARS model

Factors	GCV	RSS
Land use	100	100
Geomorphology	79.8	85.3
Slope	76.3	79.2
Soil	74.8	68.7
Lithology	71.1	55.4
NDVI	57.9	53.6
Source: Study findings		

The OOB results show a predicted error rate of about 22.17%. The accuracy of the model can be considered 77.83%. Based on the results of Table 4, on the one hand, the model incorrectly predicted 9 cases in the absence of DSA (row 1) in the presence of DSA (error 1) and the section Existence of DSA predicted 11 cases in the column of the absence of DSA (error 2). On the other hand, the model correctly predicted the absence of DSA for 97 cases and the presence of DSA for 95 cases.

Figure 6. Mean accuracy reduction and Gini mean reduction using the random forest model.

The results of the MARS method were used to evaluate the factors affecting the establishment of dust collection centers. The main difference between this method and conventional methods is that the predictive model while determining the effective variables, determines the dependent variable versus the independent variable. To apply the MARS analysis, the model is first fitted to the data with different

settings. These settings include the maximum number of base functions in the advanced stage, the maximum order of interactions, and the smoothing parameter. It should be noted that the maximum number of base functions, as well as the maximum order of interactions, are parameters that are determined by the user. In the MARS model, in the advanced stage, all the basic functions are added to the model step by step, and at the end of this stage, the generated model causes a high computational error.. In the regression stage, we achieved the final model by removing the redundant base functions that have the least effect on creating DSA. With each adjustment, a model is estimated and the chosen the best model is determined based on the minimum squares of the estimation error (RSS) and the GCV value. These results were calculated using the earth function in the R software. The MARS model was optimized with 11 nodes out of 23 nodes containing 12 base functions with GCV: 0.1 and also 18 subcategories out of 29 subcategories of independent variables. The MARS model uses only the independent variables and removes the other variables.

The MARS model also can analyze susceptibility by distinguishing between high-impact variables and low-impact variables using the GCV (generalized cross-validation) and RSS (sum of squares of error) and by determining the degree of importance of each. Table 5 shows the ineffective variables and the results of determining the degree of the importance of the effective variables. Figure 2 shows the relative contribution of each of the input parameters of the model in terms of the GCV.

The results indicate the 100% relative participation of the land use variable in the construction of the final model. The RSS value for land use is 100, which indicates that if land use is removed from the model, the sum of the squares of the error is the maximum. Therefore, the existence of this variable is very important and shows that land use has a major and more effective role than other variables in creating DSA. Other variables including geomorphology, slope, soil, lithology, and NDVI are in the next categories in terms of importance and impact. These results are not consistent with the study of Gholami et al. (2020) which assessed the impact of land use on dust at a moderate level in Khuzestan province, but this study is in line with the study of Boroughani et al (2020). Also, the results of this study are consistent with the results of Rahmati et al. (2020) whose research indicated that soil map and land use have the greatest impact and in contrast to factors such as geology and topography have the least impact on the modeling of dust sources.

3.3 Dust source susceptibility mapping (DSSM)

After executing the models in the R software for observational data and generalizing the modeling process to the whole study area, the output is a file with two columns of numbers zero and one. The zero column means no DSA for each pixel and column one indicates the existence of DSA for each pixel. DSSM modeling results were converted to point files based on the coordinates of each pixel in the GIS software environment. Then, the final map was prepared from a point-to-raster format. Finally, based natural fractures were classified into 4 classes' low, medium, high, and very high susceptibility. (Fig. 7). To determine the overall status of the case study, the area of dust sensitivity classes was calculated. Figures (8) shows the area of each sensitivity class and the percentage of DSA validation of the dust source susceptibility map.

Figure 7. DSSMs are produced by RF, MARS, and LR models.

The results of the LR algorithm showed that 7.8% of the research area is in the low susceptibility area and more than 68% is in the very high susceptibility area. The results also indicated that most of the DSA (81.6%) are in the areas with high susceptibility. Based on the results more than 88% of DSA were placed in areas with high and very high susceptibility. Examination of the class area of the dust susceptibility map using an RF algorithm showed that in the classes with very high susceptibility, about 70% of the DSA were located at the class level. The MARS model also showed that more than 80% of the DSA were placed in two classes of high and very high susceptibility.

It was also shown that in all three models, high and very high susceptibility classes generally covered a large percentage of the research area. The highest percentage of DSA was also in this susceptibility category. In the RF and March model, very sensitive layers generally covered a smaller percentage of the case study. Compared to the LR model, the percentage of DSA in the high sensitivity class was higher in the MARS and RF models, which indicates higher accuracy and more accurate implementation of these two models compared to the LR model.

Figure 8. Percentage of the area of sensitivity classes and percentage of the number of dust sources in the validation stage

Validation of prepared maps is an essential step in the development and identification of sensitive areas and their sources (Crawford et al., 2021). In this research, 30% of the DSA were used for the evaluation or testing phase (called the prediction rate), and 70% of the DSA were used for the modeling or training phase (called the success rate). As mentioned, to validate the models used, the ROC curve and the area under the AUC curve and RMSE were used for evaluation. The validation results of the models used in the test data (test, 30%) showed that the RF, MARS, and LR models had sub-curved levels of 0.94, 0.89, and 0.78, respectively. In addition, the validation results of these models using the training data showed the sub-curves of 0.92, 0.86, and 0.76 for the RF, MARS, and LR models, respectively. This is consistent with previous studies in that they also identified an RF with higher accuracy than other machine learning models for the spatial modeling of dust emission risks and source identifications (Boroughani et al., 2020; Ebrahimi-Khusfi et al., 2021; Gholami et al., 2019). The result is also consistent with Rahmati et al research (2020) that identified sources of dust aerosol using a new framework based on remote sensing and modeling. Our results showed that the highest potential source of dust detected by the RF is in eastern Iran. Based on the RMSE, it was found that the performance of the RF model was significantly higher than the other models. Table 6 shows the area under the curve and root mean square error values in the training and validation phases of all the models and Fig. 9 shows the evaluation results of the models.

Table 6
Area under the curve (AUC) and root mean square error (RMSE) values in the training and validation phases all of the models

Phases	Models	AUC (%)	RMSE
Training	RF	94	0.021
	MARS	89	0.032
	LR	78	0.05
Validation	RF	92	0.038
	MARS	86	0.062
	LR	76	0.078
Source: Study findings			

Figure 9. (1) The success rate curve and (2) the predictive rate curve for the susceptibility maps produced in this research for all models

Source: Study findings

Like any other study, this study had some limitations. As the study area was located in Iran and Iraq, it was very difficult to prepare effective layers because the scales and preparation methods were different in each country.

4. Conclusion

The goal of this research was to integrate remote sensing and machine learning techniques for spatial mapping of the earth's sensitivity to dust diffusion in a very important DSA in Iran and Iraq. For this purpose, DSA was identified using MODIS satellite images and the Miller method, and then, prioritizing the effective factors and dust source susceptibility maps using LR methods, MARS, and RF was addressed. For this purpose, six independent variables including soil, lithology, slope, vegetation index, geomorphology units, and land use were used as effective factors in creating the DSA. The results of the MARS, RF, and LR models showed that the highest percentage of the DSA was in the very sensitive class. The results of the implementation of all three models also showed that the land use factor had the greatest impact on dust vulnerability in the study area and the NDVI had less impact than other factors. Evaluation of the models using the ROC method showed that the RF model was in the excellent category, the LR model was in the good category, and the MARS model was in the very good category. The RF with an area under the AUC curve of 0.94 had a higher performance than the other two methods for evaluation. The performance of the RF model was significantly higher than the other models based on

the RMSE. The results of this research showed that climate change, drought, the war in the region and military operations, surface water control, diversion of rivers, and dam projects have caused a large part of the region to become highly sensitive to dust. The results of this model can be useful for planners and managers to control and reduce the risk of negative dust consequences. It is also recommended to prepare spatial maps of various environmental hazards, especially wind erosion and predict the sensitivity of the earth to dust emissions. Given the high potential impact of dust particles in many parts of Iran, we suggest that in the future, research on dust source sensitivity maps be extended to other regions.

Declarations

Conflict of Interest

The authors declare that there is no conflict of interests regarding the publication of this article.

Availability of data and materials

The data that support the findings of this study are available from the corresponding author, Mohammad Ali Zangane Asadi, upon reasonable request.

Funding

This work was supported by Mohammad Ali Zangane Asadi (Grant) from Hakim Sabzevari University

Authors Contributions

All authors contributed to the study conception and design. Material preparation, data collection and analysis were performed by Sima Pourhashemi, Mohammad Ali Zangane Asadi and Mahdi Boroughani. The first draft of the manuscript was written by Sima Pourhashemi and Mahdi Boroughani and all authors commented on previous versions of the manuscript. All authors read and approved the final manuscript.

Ethics approval and consent to participate

Not applicable.

Consent for publication

The authors have not submitted the manuscript to a preprint server before submitting it to Environmental Science and Pollution Research. We confirm that this manuscript has not been published elsewhere and is not under consideration by another journal. All authors have approved the manuscript and agreed with its submission to Environmental Science and Pollution Research.

References

1. Abyat A, Azhdari A, Kia HA, Joudaki M (2019) Khuzestan plain continental sabkhas, southwest Iran. Carbonates Evaporites 34(4):1469–1487
2. Akbari M, Bashiri M, Rangavar A (2017) Application of Data Mining Algorithms to Appreciate Sensitivity and Spatial Zoning Prone to Floating View in Khorasan Razavi Display Basins. J Environ Eros Res 7(26):16–42
3. Al-Dousari A, Doronzo D, Ahmed M (2017) Types, indications and impact evaluation of sand and dust storms trajectories in the Arabian Gulf. Sustainability 9(9):1526
4. Alilou H, Rahmati O, Singh VP, Choubin B, Pradhan B, Keesstra S, Sadeghi SH (2019) Evaluation of watershed health using Fuzzy-ANP approach considering geo-environmental and topo-hydrological criteria. J Environ Manage 232:22–36
5. Arabameri A, Pal C, Rezaie S, Chakrabortty F, Saha R, Blaschke A, Di Napoli T, Ghorbanzadeh M, Ngo T, P.T (2021) Decision tree based ensemble machine learning approaches for landslide susceptibility mapping.Geocarto International, pp.1–35
6. Arkian F (2017) Long-term variations of aerosols concentration over ten populated cities in iran based on satellite data. Hydrol Curr Res 8 https://doi.org/10.4172/2157- 7587.1000274
7. Baddock MC, Ginoux P, Bullard JE, Gill TE (2016) Do MODIS-defined dust sources have a geomorphological signature? Geophys. Res Lett 43(6):2606–2613
8. Boloorani AD, Kazemi Y, Sadeghi A, Shorabeh SN, Argany M (2020) Identification of dust sources using long term satellite and climatic data: A case study of Tigris and Euphrates basin. Atmos Environ. doi.org/10.1016/j.atmosenv.2020.117299
9. Boroughani M, Hashemi H, Hosseini SH, Pourhashemi S, Berndtsson R (2019) Desiccating Lake Urmia: a new dust source of regional importance. IEEE Geosci Remote Sens Lett 17(9):1483–1487
10. Boroughani M, Pourhashemi S, Hashemi H, Salehi M, Amirahmadi A, Asadi MAZ, Berndtsson R (2020) Application of remote sensing techniques and machine learning algorithms in dust source detection and dust source susceptibility mapping. Ecol Inf 56:101059
11. Boroughani M, Pourhashemi S, Gholami H, Kaskaoutis DG (2021) Predicting of dust storm source by combining remote sensing, statistic-based predictive models and game theory in the Sistan watershed, southwestern Asia. J Arid Land 13(11):1103–1121
12. Boroughani M, Mohammadi M, Mirchooli F, Fiedler S (2022) Assessment of the impact of dust aerosols on crop and water loss in the Great Salt Desert in Iran. Comput Electron Agric 192:106605
13. Cao H, Liu J, Wang G, Yang G, Luo L (2015) Identification of sand and dust storm source areas in Iran. J Arid Land 7(5):567–578
14. Chaudhary A, Bhupendra MSh, Gopal SA S. R (2021) Ageratina adenophora and Lantana camara in Kailash Sacred Landscape, India: Current distribution and future climatic scenarios through modeling. PLoS ONE 16(5):e0239690
15. Chen X, Chen W (2021) GIS-based landslide susceptibility assessment using optimized hybrid machine learning methods. CATENA 196:104833

16. Crawford MM, Dortch JM, Koch HJ, Killen AA, Zhu J, Zhu Y, Haneberg WC (2021) Using landslide-inventory mapping for a combined bagged-trees and logistic-regression approach to determining landslide susceptibility in eastern Kentucky, USA.Quarterly Journal of Engineering Geology and Hydrogeology, 54(4)
17. Dube F, Nhapi I, Murwira A, Gumindoga W, Goldin J, Mashauri DA (2014) Potential of weight of evidence modelling for gully erosion hazard assessment in Mbire District–Zimbabwe, vol 67. Physics and Chemistry of the Earth, Parts A/B/C, pp 145–152
18. Ebrahimi-Khusfi Z, Nafarzadegan AR, F., Dargahian (2021) Predicting the number of dusty days around the desert wetlands in southeastern Iran using feature selection and machine learning techniques. Ecol Ind 125. https://doi.org/10.1016/j.ecolind.2021.107499
19. Feng C, Janssen H (2018) Hygric properties of porous building materials (III): Impact factors and data processing methods of the capillary absorption test. Build Environ 134:21–34
20. Feuerstein S, Schepanski K (2019) Identification of dust sources in a Saharan dust hotspot and their implementation in a dust-emission model. Remote Sens 11(1):4
21. Francis D, Chaboureau J-P, Nelli N, Cuesta J, Alshamsi N, Temimi M, Pauluis O, Xue L (2021) Summertime dust storms over the Arabian Peninsula and impacts on radiation, circulation, cloud development and rain. Atmos Res 250:105364. https://doi.org/10.1016/j.atmosres.2020.105364
22. Francis DBK, Flamant C, Chaboureau JP, Banks J, Cuesta J, Brindley H, Oolman L (2017) Dust emission and transport over Iraq associated with the summer Shamal winds, vol 24. Aeolian Research, pp 15–31
23. Friedman JH (1991) Multivariate Adaptive Regression Splines. The Annals of Statistics 19:1–67
24. Genuer R, Poggi J-M, Tuleau-Malot C, Villa-Vialaneix N (2017) Random forests for big data. Big Data Res 9:28–46
25. Gholami H, Mohamadifar A, Collins AL (2020) Spatial mapping of the provenance of storm dust: Application of data mining and ensemble modelling. Atmos Res 233:104716
26. Gholami H, Mohammadifar A, Collins AL (2019) Spatial mapping of the provenance of storm dust: Application of data mining and ensemble modelling Hamid. Atmos Res 104716. https://doi.org/10.1016/j.atmosres.2019.104716
27. Giang PQ, Trang NTM, Anh TTH, Binh NT (2020) Prediction of economic loss of rice production due to flood inundation under climate change impacts using a modeling approach: A case study in Ha Tinh Province. Vietnam Clim Chang 6:52–63
28. Gomila R (2021) Logistic or linear? Estimating causal effects of experimental treatments on binary outcomes using regression analysis. J Exp Psychol Gen 150(4):700
29. Goossens D, Buck B (2014) Dynamics of dust clouds produced by off-road vehicle driving. J Earth Sci Geotech Eng 4(2):1–21
30. Guo P, Lam J, Li V (2018) A novel machine learning approach for identifying the drivers of domestic electricity users' price responsiveness

31. Hao C, Yunus AP, Subramanian SS, Avtar R (2021) Basin-wide flood depth and exposure mapping from SAR images and machine learning models. Journal of Environmental Management, 297, p.113367
32. Hassangavyar MB, Damaneh HE, Pham QB, Linh NTT, Tiefenbacher J, Bach QV (2020) Evaluation of re-sampling methods on performance of machine learning models to predict landslide susceptibility. Geocarto International, pp 1–23
33. Hassangavyar MB, Damaneh HE, Pham QB, Linh NTT, Tiefenbacher J, Bach QV (2020) Evaluation of re-sampling methods on performance of machine learning models to predict landslide susceptibility. Geocarto International, pp 1–23
34. Heidarian P, Azhdari A, Joudaki M, Khatooni JD, Firoozjaei SF (2018) Integrating remote sensing, GIS, and sedimentology techniques for identifying dust storm sources: a case study in Khuzestan. Iran J Indian Soc Remote Sens 46(7):1113–1124
35. Hong H, Naghibi SA, Pourghasemi HR, Pradhan B (2016) GIS-based landslide spatial modeling in Ganzhou City, China. Arab. J. Geosci. 9 (2), 1–26.10.1007%2Fs12517-015-2094-y
36. Javadian M, Behrangi A, Sorooshian A (2019) Impact of drought on dust storms: case study over Southwest Iran. Environ Res Lett 14(12):124029
37. Jiang C, Fan W, Yu N, Liu E (2021) Spatial modeling of gully head erosion on the Loess Plateau using a certainty factor and random forest model. Sci Total Environ 783:147040
38. Jiao P, Wang J, Chen X, Ruan J, Ye X, Alavi AH (2021) Next-generation remote sensing and prediction of sand and dust storms: State-of-the-art and future trends. Int J Remote Sens 42(14):5277–5316
39. Kandakji T, Gill T, Lee J (2021) Drought and land use/land cover impact on dust sources in Southern Great Plains and Chihuahuan Desert of the U.S.: Inferring anthropogenic effect.Science of the Total Environment, (755),1–13
40. Kandakji T, Thomas E, Jeffrey A (2020) Identifying and characterizing dust point sources in the southwestern United States using remote sensing and GIS. Geomorphology 353:107019
41. Karimi B, Samadi S (2019) Mortality and hospitalizations due to cardiovascular and respiratory diseases associated with air pollution in Iran: A systematic review and meta-analysis. Atmos Environ 198:438–447
42. Kok JF, Ridley DA, Zhou Q, Miller RL, Zhao C, Heald CL, Ward DS, Albani S, Haustein K (2017) Smaller desert dust cooling effect estimated from analysis of dust size and abundance. Nat Geosci 10(4):274–278
43. Lahjouj A, El Hmaidi A, Bouhafa K, Boufala MH (2020) Mapping specific groundwater vulnerability to nitrate using random forest: Case of Sais basin, Morocco. Model Earth Syst Environ 6(3):1451–1466
44. Lee-Sunmin Kim JC, Jung HS, Lee MJ, Lee S (2017) Spatial prediction of flood susceptibility using random-forest and boosted-tree models in Seoul metropolitan city. Korea Geomat Nat Hazard Risk 8:1185–1203
45. Lee EH, Sohn BJ (2011) Recent increasing trend in dust frequency over Mongolia and Inner Mongolia regions and its association with climate and surface condition change. Atmos Environ 45(27):4611–

4616

46. Lee JA, Gill TE, Mulligan KR, Acosta MD, Perez AE (2009) Land use/land cover and point sources of the 15 December 2003 dust storm in southwestern North America. Geomorphology 105(1–2):18–27
47. Lee J, Gill T, Mulligan K, Acosta MD, Perez A (2009) Land use/land cover and point sources of the 15 December 2003 dust storm in southwestern North America. Geomorphology 105(2):18–27. doi:10.1016/j.geomorph.2007.12.016
48. Lee J, Shi YR, Cai C, Ciren P, Wang J, Gangopadhyay A, Zhang Z (2021) Machine Learning Based Algorithms for Global Dust Aerosol Detection from Satellite Images: Inter-Comparisons and Evaluation. Remote Sens 13(3):456
49. Liu Y, Wang G, Hu Z, Shi P, Lyu Y, Zhang G, Gu Y, Liu Y, Hong C, Guo L, Hu X, Yang Y, Zhang X, Zheng H, Liu L (2020) Dust storm susceptibility on different land surface types in arid and semiarid regions of northern China. Atmos Res 243:1–10
50. Manap MA, Nampak H, Pradhan B, Lee S, Sulaiman WNA, Ramli MF (2014) Application of probabilistic-based frequency ratio model in groundwater potential Mapping Using remote sensing data and GIS. Arab J Geosci 7(2):711–724. https://doi.org/10.1007/s12517-012-0795-z
51. Martinello C, Cappadonia C, Conoscenti C, Agnesi V, Rotigliano E (2021) Optimal slope units partitioning in landslide susceptibility mapping. J Maps 17(3):152–162
52. Martinez-Garcia A, Rosell-Mele A, Jaccard SL, Geibert W, Sigman DM, Haug GH (2011) "Southern Ocean dust–climate coupling over the past four million years". Nature 476(7360):312–315
53. Miller SD (2003) A consolidated technique for enhancing desert dust storms with MODIS.Geophysical Research Letters, 30(20)
54. Miller SD (2003) A consolidated technique for enhancing desert dust storms with MODIS. Geophys. Res. Lett. 30 (20), 2071. https://doi.org/10.1029/2003GL018279
55. Martinich N, Roman J, Mickley H, L.J (2019) Effects of increasing aridity on ambient dust and public health in the US southwest under climate change. GeoHealth 3(5):127–144
56. Namdari S, Karimi N, Sorooshian A, Mohammadi G, Sehatkashani S (2018) Impacts of climate and synoptic fluctuations on dust storm activity over the Middle East. Atmos Environ 173:265–276
57. Nhu VH, Mohammadi A, Shahabi H, Ahmad BB, Al-Ansari N, Shirzadi A, Geertsema M, Kress R, Karimzadeh V, Valizadeh Kamran S, Chen W, Zou M (2020) R. Y. 2020. The random forest algorithm for statistical learning. The Stata Journal, 20(1), 3–29
58. Nobakht M, Shahgedanova M, White K (2021) New Inventory of Dust Emission Sources in Central Asia and Northwestern China Derived From MODIS Imagery Using Dust Enhancement Technique.Journal of Geophysical Research: Atmospheres, 126(4), e2020JD033382.
59. O'brien RM (2007) A caution regarding rules of thumb for variance inflation factors. Qual Quant 41(5):673–690
60. Park S, Hamm S-Y, Jeon H-T, Kim J, Sustainability (2017) 9, 1157. https://doi.org/10.3390/su9071157

61. Quevedo RP, Maciel DA, Uehara TDT, Vojtek M, Rennó CD, Pradhan B, Vojteková J, Pham QB (2021) Consideration of Spatial Heterogeneity in Landslide Susceptibility Mapping using Geographical Random Forest Model. Geocarto International, (just-accepted), pp 1–20
62. Rahmati O, Kornejady A, Deo RC (2021) Spatial prediction of landslide susceptibility using random forest algorithm. Intelligent Data Analytics for Decision-Support Systems in Hazard Mitigation. Springer, Singapore, pp 281–292
63. Rahmati O, Mohammadi F, Ghiasi SS, Tiefenbacher J, Moghaddam DD, Coulon F, Nalivan OA, Bui DT (2020) Identifying sources of dust aerosol using a new framework based on remote sensing and modelling. Sci Total Environ 737:139508
64. Rashki A, Middleton NJ, Goudie AS (2021) Dust storms in Iran – Distribution, causes, frequencies and impacts.Aeolian Research, (48):1–17
65. Roy P, Pal C, Arabameri S, Chakrabortty A, Pradhan R, Chowdhuri B, Lee I, Tien Bui D (2020) Novel ensemble of multivariate adaptive regression spline with spatial logistic regression and boosted regression tree for gully erosion susceptibility. Remote Sensing, 12(20), p.3284
66. Schepanski K, Tegen I, Macke A (2012) Comparison of satellite based observations of Saharan dust source areas. Remote Sens Environ 123:90–97
67. Schepanski K, Tegen I, Macke A (2012) Comparison of satellite based observations of Saharan dust source areas. Remote Sens Environ 123:90–97
68. Shaheen A, Wu R, Aldabash M (2020) Long-term AOD trend assessment over the Eastern Mediterranean region: A comparative study including a new merged aerosol product. Atmos Environ. doi:10.1016/j.atmosenv.2020.117736
69. Shano L, Raghuvanshi TK, Meten M (2021) Landslide Hazard Zonation using Logistic Regression Model: The Case of Shafe and Baso Catchments, Gamo Highland, Southern Ethiopia. Geotechnical and Geological Engineering, pp.1–19
70. Soni M, Payra S, Verma S (2018) Particulate matter estimation over a semi arid region Jaipur, India using satellite AOD and meteorological parameters. Atmos Poll Res. doi: 10.1016/j.apr.2018.03.001
71. Sun D, Xu J, Wen H, Wang D (2021) Assessment of landslide susceptibility mapping based on Bayesian hyperparameter optimization: A comparison between logistic regression and random forest. Eng Geol 281:105972
72. Taheri F, Forouzani M, Yazdanpanah M, Ajili A (2020) How farmers perceive the impact of dust phenomenon on agricultural production activities: A Q-methodology study. J Arid Environ 173:104028
73. Vickery K, Eckardt F (2013) Dust emission controls on the lower Kuiseb River valley, central Namib. Aeolian Res 10:125–133. https://doi.org/10.1016/j.aeolia.2013.02.006
74. Walker AL, Liu M, Miller SD, Richardson KA, Westphal DL (2009) Development of a dust source database for mesoscale forecasting in Southwest Asia. J Geophys Res 114(18):1–24. https://doi.org/10.1029/2008JD011541

75. Wang H, Zhang L, Yin K, Luo H, Li J (2021) Landslide identification using machine learning. Geosci Front 12(1):351–364
76. Wang L, Tremblay D, Zhang B, Han Y (2016) Fast and accurate collocation of the visible infrared imaging radiometer suite measurements with cross-track infrared sounder. Remote Sens 8(1):76. doi:10.3390/rs8010076
77. Wang L, Wu C, Gu X, Liu H, Mei G, Zhang W (2020) Probabilistic stability analysis of earth dam slope under transient seepage using multivariate adaptive regression splines. Bull Eng Geol Environ 79(6):2763–2775
78. Wang T, Ma H, Liu J, Luo Q, Wang Q, Zhan Y (2021) Assessing frost heave susceptibility of gravelly soils based on multivariate adaptive regression splines model. Cold Reg Sci Technol 181:103182
79. Wu C, Lin Z, He J, Zhang M, Liu X, Zhang R, Brown H (2016) A process-oriented evaluation of dust emission parameterizations in CESM: Simulation of a typical severe dust storm in E ast A sia. J Adv Model Earth Syst 8(3):1432–1452
80. Wu H, Lin A, Xing X, Song D, Li Y (2021) Identifying core driving factors of urban land use change from global land cover products and POI data using the random forest method. Int J Appl Earth Obs Geoinf 103:102475
81. Yang R-M, Zhang G-L, Liu F, Lu Y-Y, Yang F, Yang F, Yang M, Zhao Y-G, Li D-C (2016) Comparison
82. Yang L, Jin S, Danielson P, Homer C, Gass L, Bender SM, Case A, Costello C, Dewitz J, Fry J, Funk M, Granneman B, Liknes GC, Rigge M, Xian G (2018) A new generation of the United States National Land Cover Database: requirements, research priorities, design, and implementation strategies. ISPRS J. Photogramm. Remote Sens. 146, 108–123
83. Yu H, Chin M, Yuan T, Hremer B, Prospero LA, Omar JM, Winker A, Yang D, Zhang Y, Zhang Y, Zhao Z, C (2015) The fertilizing role of African dust in the Amazon rainforest: a first multiyear assessment based on CALIPSO LIDAR observations. Geophys Res Lett 42:1984–1991
84. Zhang S, Li C, Peng J, Peng D, Xu Q, Zhang Q, Bate B (2021) GIS-based soil planar slide susceptibility mapping using logistic regression and neural networks: a typical red mudstone area in southwest China. Geomatics, Natural Hazards and Risk, 12(1), 852–879
85. Zhang X, Kang T, Wang H, Sun Y (2010) Analysis on spatial structure of land use change based on remote sensing and geographical information system. Int J Appl Earth Obs Geoinf 12:S145–S150

Figures

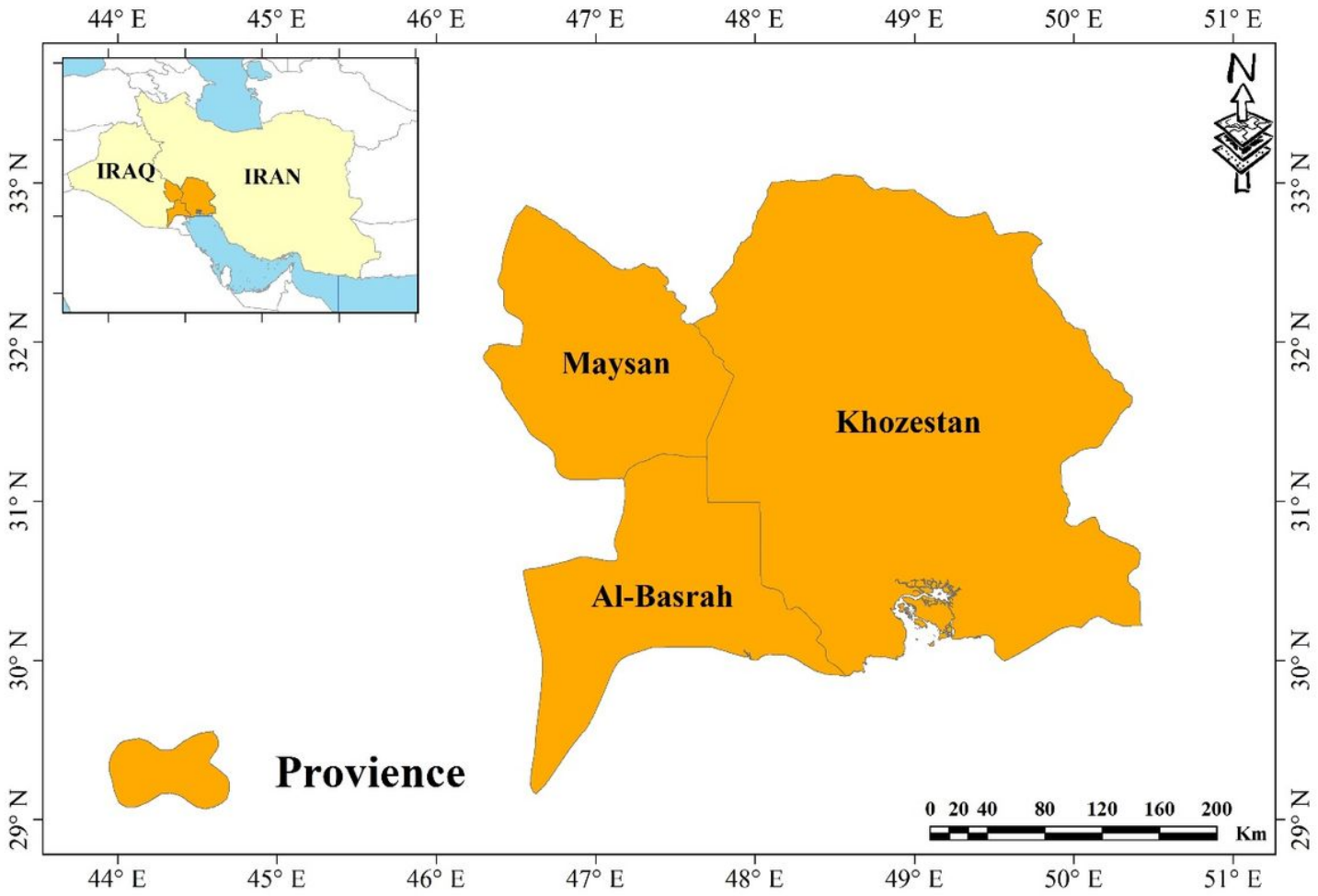

Figure 1

Location of the case study

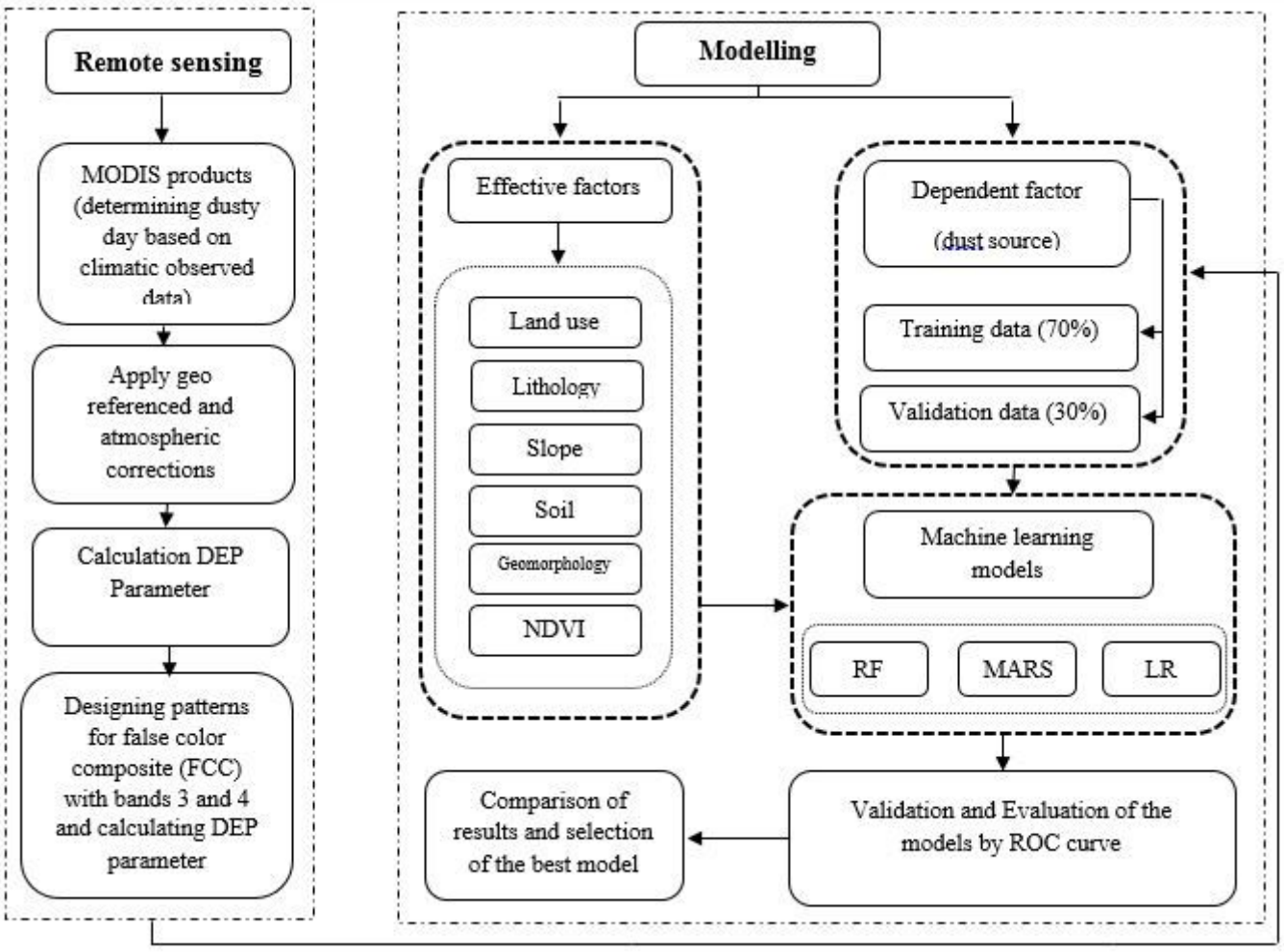

Figure 2

Flow chart for preparation of dust susceptibility maps using Logistic Regression, MARS, and Random Forest models

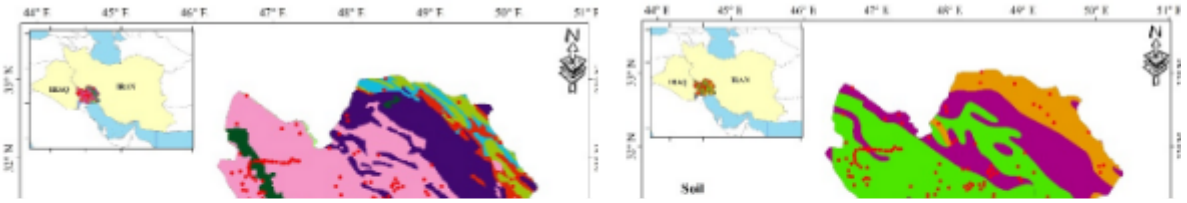

Figure 3

Map of effective factors of dust source

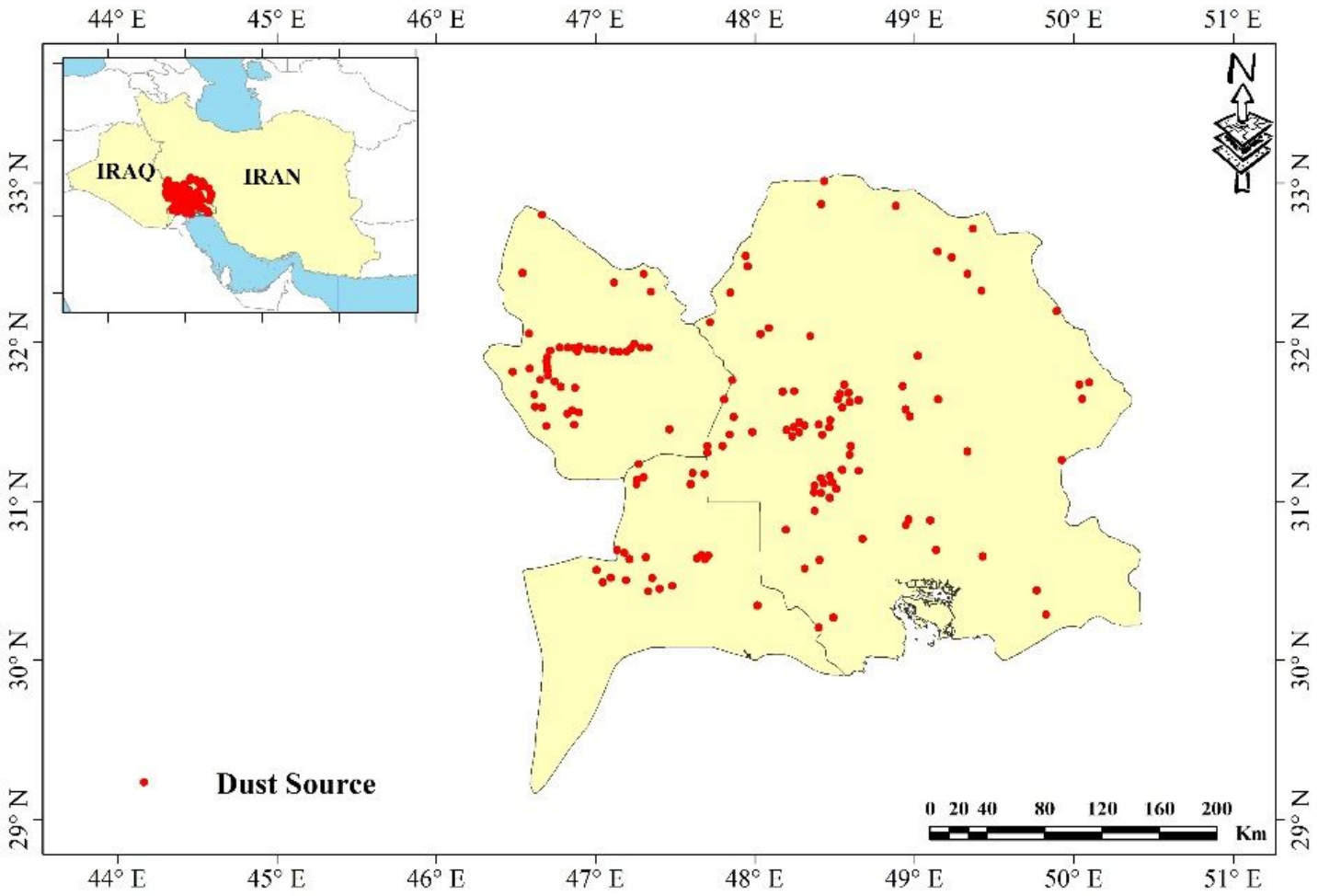

Figure 4

Distribution of dust sources points identified

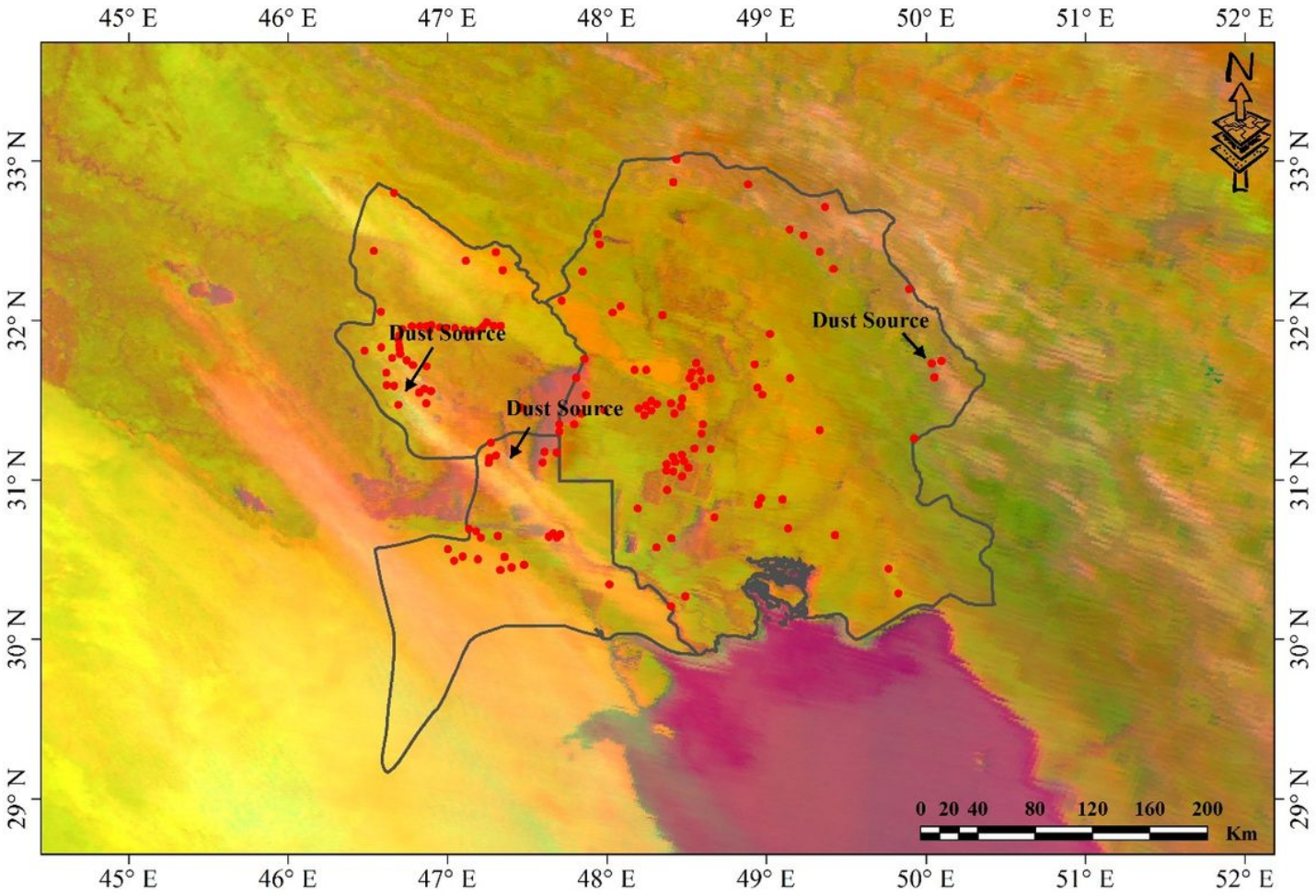

Figure 5

An example of dust storm detection in the case study from MODIS satellite Imagery with FCC (R: DEP, G: B4, B: B3)

Figure 6

Mean accuracy reduction and Gini mean reduction using random forest model.

Figure 7

DSSMs produced by RF, MARS, and LR model.

Figure 8

Percentage of area of sensitivity classes and percentage of number of dust source in validation stage

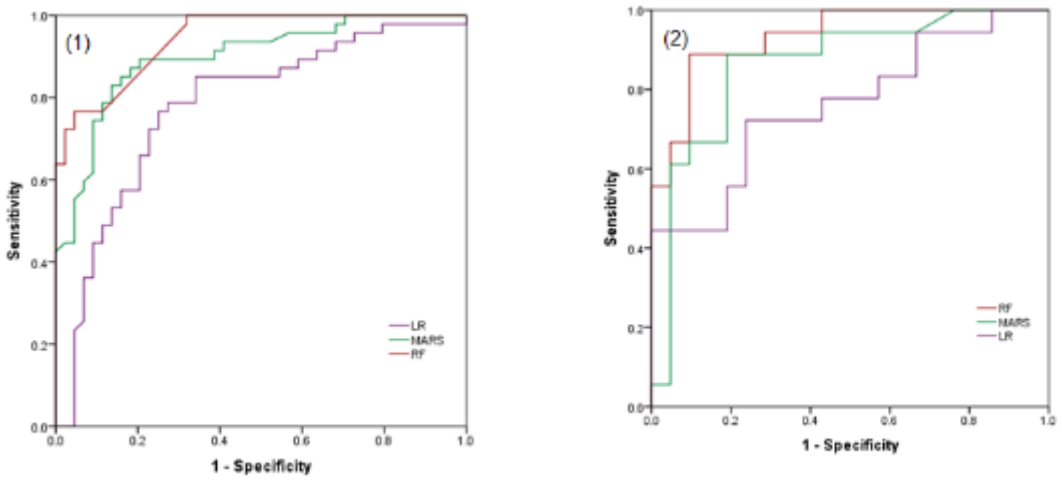

Figure 9

(1) The success rate curve and (2) the predictive rate curve for the susceptibility maps produced in this research for all models